88-Inch Cyclotron: The One-Stop Facility for Electronics Radiation Testing

Michel Kireeff Covo*, Robert A. Albright, Brien F. Ninemire, Michael B. Johnson, Adrian Hodgkinson, Tim Loew, Janilee Y. Benitez, Damon S. Todd, Daniel Z. Xie, Thomas Perry, and Larry Phair
88- Inch Cyclotron
Lawrence Berkeley National Laboratory
1 Cyclotron Road, Berkeley, California 94720, USA
*mkireeffcovo@lbl.gov

D. L. Bleuel
Lawrence Livermore National Laboratory,
Livermore, California 94550, USA

K. P. Harrig, B. L. Goldblum, J. A. Brown, T. Laplace, J. Bevins, M. Harasty, E. F. Matthews, and L. A. Bernstein
Department of Nuclear Engineering,
University of California,
4155 Etcheverry Hall, MC 1730, Berkeley, California 94720, USA

Adam Bushmaker
Physical Sciences Laboratories
The Aerospace Corporation
355 S. Douglas Street, El Segundo, California 90245, USA.

***Abstract*— In the outer space down to the altitudes routinely flown by the larger commercial aircrafts, radiation is a serious problem for the microelectronics circuits. The 88-Inch Cyclotron at Lawrence Berkeley National Laboratory is a sector-focused cyclotron and is the home of the Berkeley Accelerator Space Effects Facility, where the effects of energetic particles on sensitive microelectronics are studied with the goal of designing electronic systems for the space community. The paper will describe the flexibility of the facility and its capabilities for testing the bombardment of the electronics by heavy ions, light ions, and neutrons.**

Keywords—Radiation Hardening; Single Event Effects; Ion Beam; Neutron Beam; Cyclotron; ECR

I. Introduction

The atmosphere and the Earth's magnetic field shield the Earth's surface from most of the ionizing radiation that originates from the Sun and other stars.

The solar wind boils continuously off the Sun and is constituted of 80% protons, 18% alpha particles, and traces of heavier charged particles [1]. It has a similar composition to the galactic cosmic rays that originate outside the solar system. Occasionally, however, a magnetic disturbance in the Sun results in an explosive ejection of huge amounts of matter from the solar corona, known as coronal mass ejection, which is responsible for showers of high energy particles impacting Earth's atmosphere within 15-20 minutes of the event [2].

The first spacecrafts lost due to total radiation dose effects occurred unexpectedly in 1962. Telstar and six other satellites were lost within a seven-month period after a high altitude nuclear weapon test produced a large number of beta particles, which caused a new and very intense radiation belt lasting until the early 1970's [3].

When high-energy ions enter a material, they lose energy to the medium. The energy loss from the projectile per unit path length is known as stopping power, which has two components, the nuclear and the electronic.

The nuclear stopping power is caused by elastic collisions with the nuclei of the target material. The electronic stopping power is produced by inelastic collisions with the electrons [4]. Electronic stopping power is practically equivalent to the linear energy transfer (LET) for the ions produced by the cyclotron.

The energy deposited from the electronic stopping power produces a dense track of electron-hole pairs along the ion track by the ionization process. If the ion interacts with an electronic semiconductor component, some charge will be collected at the p-n junction, while others will recombine [5]. As a result, a very short duration current pulse is generated at the circuit node, which can produce transient effects such as single-event upset and multiple-bit upset, catastrophic events with single-event latch-up and snapback, and single-event hard errors [6]. Long term material degradation may be produced by charge collected and annealing, or by displacement damage caused by nuclear stopping power.

Knowledge of the mechanisms underlying the radiation response of electronic devices is of paramount importance for devising hardness assurance methodologies to guarantee that the tested devices can work reliably, and developing radiation hardened circuits and design techniques to improve the tolerance of electronic circuits to specific effects of radiation.

Because the loss of a piece of equipment in space can be very costly, scientists and engineers from the aerospace industry, NASA and the Department of Defense perform radiation effects studies using accelerators.

Ions have a property of depositing energy mainly at the Bragg peak, immediately before coming to rest; therefore, they can be used to probe isolated parts of electronic devices.

The paper discusses the capabilities of the 88-Inch Cyclotron, which is the home of the Berkeley Accelerator Space Effects (BASE) Facility, to provide well-characterized beams of neutrons, heavy ions, and light ions that simulate the space environment [7].

This work was supported by the Director, Office of Science, Office of Nuclear Physics, Division of Nuclear Physics, U.S. Department of Energy under Contract No. DE-AC02-05CH11231.
978-1-5090-4234-0/17/$31.00 ©2017 IEEE

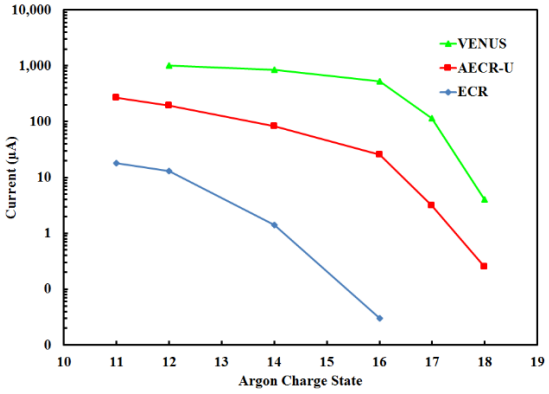

Fig. 1. Currents versus charge state produced by ECR, AECR-U, and VENUS sources.

II. Electron Cyclotron Resonance Ions Sources

The cyclotron has three ion sources that have led to progressively higher intensities and charge states of heavier ions. The first generation of electron cyclotron resonance (ECR) ion source was coupled to the cyclotron in the early 1980s. It has a 6.4 GHz Klystron that generates 2.5 kW of power and provides the primary heating frequency. In conventional ECR sources [8], the ECR zones are usually thin annular, ellipsoidal-shaped surfaces which surround the optical axis of the source. The ECR magnetic field for confinement is less than 0.4 T.

Geller's scaling law [9] predicts that the density of the plasma is directly proportional to the RF frequency squared, so it encourages to increase the frequency with the consequent rise of the magnetic field.

The second generation, the Advanced ECR - Upgrade ion source (AECR-U), was built and upgraded in the 1990s with maximum confinement magnetic field of 1.7 T [10]. It has one 14 GHz Klystron that generates 2.5 kW of power and provides the primary heating frequency and a 10.75 to 12.75 GHz Traveling-Wave Tube (TWT) amplifier that generates 400 W of RF power and provides the secondary heating frequency. The TWT, installed in 2010, replaced a Klystron amplifier with the goal of further optimizing the source performance [11].

The third generation, the superconducting ECR source named Versatile Ecr ion source for Nuclear Science (VENUS), was operational in early 2000s [12]. It has a 18 GHz Klystron, that provides 2.5 kW of power for the primary heating frequency, and a 28 GHz Gyrotron, that provides 10 kW of power for the secondary heating frequency. The magnetic confinement field is 4 T. VENUS can deliver high current and medium and high charge state beams and is considered among the most powerful superconducting ECR ion source in the world.

Fig. 1 shows the Argon current obtained from each source versus the charge state.

The feasibility studies for a fourth generation of ECR ion source, called Mixed Axial and Radial field System - Demonstration (MARS-D), are underway. The operating frequency will be 45 GHz with a confinement field of 6T [13].

III. 88-Inch Cyclotron and the "Cocktail" of Ions

Ions produced by ECR ion sources are injected inside the 88-Inch Cyclotron. After the ions enter the cyclotron, they are accelerated by a radiofrequency (RF) electric field and held to a spiral trajectory by a static magnetic field. The RF fields cause the ions to bunch up into packets. The ions gain velocity and the orbit increases with radius. The ions that are not synchronized with the RF are lost.

In order to improve the cyclotron efficiency, the innermost trim coil 1 and 15 were modified in 2013-14 to provide a current unbalance and alter the center region magnetic field strength, producing a magnetic mirror effect that offsets and displaces the beam axially [14].

The cyclotron operates in the frequency range of 5.5 to 16.5 MHz, but it can operate using harmonic acceleration, so the energy range of the machine is limited only by the capabilities of the magnet, not the RF system.

It was realized earlier that the variable frequency of the cyclotron translated to a mass resolution of 1/3000, meaning that the cyclotron could separate most ions of near identical mass-to-charge ratio emanating from the ion source [15]. Therefore, the combination of cyclotron and ECR sources provide the unique ability to run "cocktails" of ions. A cocktail is a mixture of ions of near-identical charge-to-mass ratio [16]. The current heavy ion cocktails available are the 4.5, 10, 16, and 30 MeV/u.

During the cyclotron operation, the ions are tuned out of the source simultaneously and the cyclotron acts as a charge-to-mass analyzer to separate them and provide different ion species and charge states for energy variable experiments, which take advantage of the different stopping power and range of ions into the components under examination.

The wideband driven RF system for the cyclotron provides fast beam tuning, allowing users to switch back and forth between several ion species of the same cocktail with small adjustments of the accelerator frequency, so a new beam does not require retuning the whole accelerator and is accomplished in approximately one minute.

During operation, a nondestructive beam current monitor, mounted after the deflectors and commissioned in 2014, can monitor the beam current. It has exceptional resolution, long term stability, and can measure the beam current leaving the cyclotron as low as 1 nA [17].

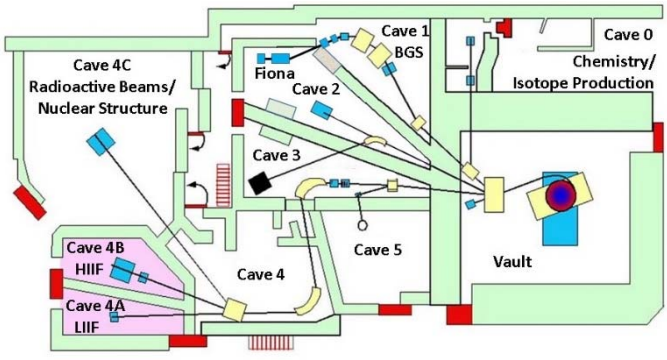

Fig. 2. Layout of the 88-Inch Cyclotron Facility.

The cyclotron has five experimental caves, Fig. 2. Cave 0 research is mainly for chemistry and isotope production. Cave 4A and 4B, part of the Berkeley Accelerator Space Effects (BASE), are a light-ion irradiation facility and heavy ion irradiation facility, respectively. Cave 4C is used for Radioactive Beams and Nuclear structure experiments and it is the cave where the world's most sensitive Gamma-Ray detector, GRETINA [18], was commissioned. Cave 1 has the Berkeley Gas-filled Separator (BGS) used for chemistry and physics research of the heaviest elements [19]. The by-products of BGS go to a recently commissioned gas catcher, RF quadrupoles, and an acceleration region before entering Cave 2 and reaching Facility for Identification of Nuclide A (FIONA) isotope separator [20]. Caves 3, 4, and 5 currently do not have any ongoing experiments.

IV. BASE FACILITY

The layout of the 88-Inch Cyclotron facility, Fig. 2, shows the BASE facility at the shaded lower left side.

A. Heavy Ion Irradiation Facility (HIIF)

The Heavy Ion Irradiation Facility (HIIF) testing takes place in the vacuum chamber located in Cave 4B. Four heavy ion cocktails regularly available (4.5, 10, 16 and 30 AmeV) are summarized in TABLE I. Depending on the cocktail, LETs from 1 to 100 MeV/mg/cm^2, range from 40 µm to 1400 µm, and flux levels of up to 10^7 ions/cm^2/sec are available.

The control room operator tunes the cyclotron frequency to select only the desired ion, a process that takes about 2 minutes.

To tune the beam into the cave, the beam is first evenly spread out to a circle of 5 cm diameter on the cave phosphor and viewed with a digital camera. Then the beam is attenuated and five Hamamatsu R647 photomultiplier tubes (PMTs) are inserted. Four PMTs are placed around the edge of the beam, and one is placed in the middle. These PMTs are then calibrated, after which the center PMT is removed to permit exposure of the target.

The PMT signal is sent up to a computer. The beam may be stopped manually or by setting run time, fluence, or effective fluence limits.

Parts tested can be remotely positioned horizontally, vertically, or rotationally with a motion table inside the vacuum chamber. An alignment laser is available to ensure the part is in the center of the beam.

B. Light Ion Irradiation Facility (LIIF)

The Light Ion Irradiation Facility (LIIF) is located in Cave 4A and it is set up to run samples in air. Beam particles are tuned to a 10 cm diameter and they travel through a nitrogen-filled ion chamber, where they leave a trail of electrons that are collected by four quadrant concentric electrodes with diameters of 1 cm, 2 cm, 4 cm, 6 cm, and 8 cm. After the beam has achieved proper uniformity, a collimator with diameters of 2.5, 5, 7.5, or 10 cm is placed on the ion chamber and an exposure is made with Gafchromic film and scanned.

TABLE I. 4.5, 10, 16 AND 30 AMEV ION COCKTAILS

Ion	Cocktail (AMeV)	Energy (MeV)	Z	A	Chg. State	% Nat. Abund.	LET 0° (MeV/mg/cm^2)	Range (µm)
B	4.5	44.90	5	10	+2	2.0E+01	**1.65**	78.5
N	4.5	67.44	7	15	+3	3.7E-01	**3.08**	67.8
Ne	4.5	89.95	10	20	+4	9.0E+01	**5.77**	53.1
Si	4.5	139.61	14	29	+6	4.7E+00	**9.28**	52.4
Ar	4.5	180.00	18	40	+8	1.0E+02	**14.32**	48.3
V	4.5	221.00	23	51	+10	1.0E+02	**21.68**	42.5
Cu	4.5	301.79	29	63	+13	6.9E+01	**29.33**	45.6
Kr	4.5	378.11	36	86	+17	1.7E+01	**39.25**	42.4
Y	4.5	409.58	39	89	+18	1.0E+02	**45.58**	45.8
Ag	4.5	499.50	47	109	+22	4.8E+01	**58.18**	46.3
Xe	4.5	602.90	54	136	+27	8.9E+00	**68.84**	48.3
Tb	4.5	724.17	65	159	+32	1.0E+02	**77.52**	52.4
Ta	4.5	805.02	73	181	+36	1.0E+02	**87.15**	53.0
Bi*	4.5	904.16	83	209	+41	1.0E+02	**99.74**	52.9
B	10	108.01	5	11	+3	8.0E+01	**0.89**	305.7
O	10	183.47	8	18	+5	2.0E-01	**2.19**	226.4
Ne	10	216.28	10	22	+6	9.3E+00	**3.49**	174.6
Si	10	291.77	14	29	+8	4.7E+00	**6.09**	141.7
Ar	10	400.00	18	40	+11	1.0E+02	**9.74**	130.1
V	10	508.27	23	51	+14	1.0E+02	**14.59**	113.4
Cu	10	659.19	29	65	+18	3.1E+01	**21.17**	108.0
Kr	10	885.59	36	86	+24	1.7E+01	**30.86**	109.9
Y	10	928.49	39	89	+25	1.0E+02	**34.73**	102.2
Ag	10	1039.42	47	107	+29	5.2E+01	**48.15**	90.0
Xe	10	1232.55	54	124	+34	1.0E-01	**58.78**	90.0
Au*	10	1955.87	79	197	+54	1.0E+02	**85.76**	105.9
He*	16	43.46	2	3	+1	1.3E-04	**0.11**	1020.0
N	16	233.75	7	14	+5	1.0E+02	**1.16**	505.9
O	16	277.33	8	17	+6	4.0E-02	**1.54**	462.4
Ne	16	321.00	10	20	+7	9.0E+01	**2.39**	347.9
Si	16	452.10	14	29	+10	4.7E+00	**4.56**	274.3
Cl	16	539.51	17	35	+12	7.6E+01	**6.61**	233.6
Ar	16	642.36	18	40	+14	1.0E+02	**7.27**	255.6
V	16	832.84	23	51	+18	1.0E+02	**10.90**	225.8
Cu	16	1007.34	29	63	+22	6.9E+01	**16.53**	190.3
Kr	16	1225.54	36	78	+27	3.5E-01	**24.98**	165.4
Xe*	16	1954.71	54	124	+43	1.0E-01	**49.29**	147.9
N	30	425.45	7	15	+7	3.7E-01	**0.76**	1370.0
O	30	490.22	8	17	+8	4.0E-02	**0.98**	1220.0
Ne	30	620.00	10	21	+10	2.7E-01	**1.48**	1040.0
Ar	30	1046.11	18	36	+17	3.4E-01	**4.87**	578.1

* Special Request only

The final processing and indication of ion chamber data provides the user with flux and fluence values for each ring and quadrant, so fluence limits can be set to stop the beam upon reaching a threshold level.

The LIIF is capable of providing standard fluxes of up to 10^9 protons/cm^2/sec. Standard proton energies include 13.5, 20, 30, 40, 50, and 55 MeV, but it can be used with other light-ions and the light-ion cocktail. The energy loss in the ion chamber and air limits the lower energy running in this facility. If the experiment requires, lower energy protons can be run in the vacuum chamber located in cave 4B.

V. NEUTRON BEAMS

In the cyclotron, a deuteron beam hits a beryllium or tantalum thin target (125 mils) and splits up into a proton and neutron [21], because deuterons have binding energy of only 2.22 MeV.

The beryllium target provides a high yield neutron beam and the tantalum target produces a low yield to cave 0. The absolute flux is measured at the target station using standard activation foil techniques.

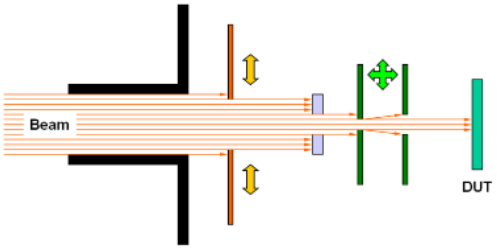

Fig. 3. Milli-Beam Schematic.

The mechanism can be explained with a simplistic Coulombic model: the deuteron deaccelerates as it approaches the target nucleus, then the proton and neutron break up at radius r and each take half of the available energy at that time.

The proton reaccelerates on the way out, leaving the neutron with an energy, $E_{neutron}$, given by

$$E_{neutron} = \frac{1}{2}\left(E_{beam} - \frac{Ze^2}{r} - 2.22\right) MeV. \qquad (1)$$

where:

E_{beam} is the deuteron beam energy;

Z is the target atomic number;

e is the elementary charge; and

r is the breakup radius.

The energy obtained in equation (1) is well defined, so this process yields a tunable forward focused neutron with an energy spread determined by the width of the breakup radius.

The energy distributions can be measured directly with a proton-recoil detector by using neutron time-of-flight (TOF) combined with pulse shape discrimination to distinguish the neutrons from the gamma-rays [22].

Quasi-monoenergetic neutron beams are available in cave 0 with tunable energies that range of from 8 to 30 MeV and fluxes of up to 10^8 neutrons/cm^2/sec. It allows studies of fusion, weapons stewardship, and radiation effects in electronics, materials damage, and biology.

The LBNL Nuclear Data Group is presently conducting detector characterization and (n,n'γ) measurements of the thick target deuteron break-up neutron source. Similar measurements are taking place at HZDR [23] and GELINA [24].

Given that the cyclotron has multi-turn extraction, the train of bunches width cannot be adjusted below few hundred nanoseconds. An effort to produce a single turn extraction is underway to space the bunches to avoid the "wrap around" effect, where slow neutrons from the previous bunch superimpose to fast neutrons from the actual bunch, allowing the measurement of the neutron time-of-flight without pilling up.

VI. Microbeam

As semiconductor parts become more miniaturized, new modes of failure appear and experimenters not only need to test whole components, but they also want to isolate and probe small sections of their electronics device under test (DUT) to pinpoint problems. Furthermore, accelerators can be used to produce pencil beams for studying the basic mechanisms contributing to single event effects (SEE).

The 88-Inch Cyclotron is unique in having beams parallel. With this goal, a series of collimators with precision slits are located inside cave 4B to produce a Milli-Beam for SEE characterization [25], shown in Fig. 3. The advanced test sub-system provides SEE spatial error isolation of approximately 10 um to 30 um minimum and up to 100 um to 300 um maximum, depending on the desired scan rate.

VII. Conclusions

In the upper layers of the atmosphere and in the outer space, radiation constitutes a serious problem for the aerospace electronics.

When high-energy ions enter a material, they lose most of the energy at the Bragg peak. As a result, an energy variable accelerator can be used to regulate the depth and amount of energy deposited to systematically test their parts in a controlled manner.

The combination of the 88-Inch Cyclotron with the ECR ion sources makes a unique device that allows switching ion species and energies in minutes. Currently, it produces 2000 hours per year of heavy and light ions, neutrons, and microbeams devoted to study transient and long lasting effects of ions impacting electronics.

The 88-Inch Cyclotron can simulate the space environment conditions that the electronics will be exposed over the years in matter of minutes. It constitutes an essential tool to develop radiation-hardened circuits and design techniques to avoid very costly loss of equipment from the aerospace industry.

Acknowledgment

The authors want to thank Craig F. Rogers, Brendan P. Cronander-Ford, Robert J. Ramer, and Mark Regis for the electronics support; Catherine R. Siero, Thomas L. Gimpel, Scott M. Small, Sierra Garret, and Nicholas M. Brickner for the operation support; and John P. Garcia, Donald Bell, and Brian D. Reynolds for the mechanical support.

References

[1] J. L. Burch, "The fury of space storms," Scientific American 2001; 284(4):86-94.

[2] D. F. Smart and M.A. Shea, "Solar radiation," In Encyclopedia of applied physics, vol. 18. New York, NY: VCH Publishers, 1997: 393-429.

[3] J. S. Mayo, H. Mann, F. J. Witt, D. S. Peck, H. K. Gummel, and W. L. Brown, "The command system malfunction of the Telstar satellite," NASA SP-32, Vol. 2, (1963), 1631-1657.

[4] M. Kireeff Covo, A. W. Molvik, A. Friedman, G. Westenskow, J. J. Barnard, R. Cohen, P. A. Seidl, J. W. Kwan, G. Logan, D. Baca, F. Bieniosek, C. M. Celata, J. L. Vay, and J. L. Vujic, "Beam energy scaling of ion-induced electron yield from K+ impact on stainless steel," Phys. Rev. ST Accel. Beams 9, 063201 (2006).

[5] F. B. McLean and T. R. Oldham, "Charge funneling in n- and p-type substrates," IEEE Trans. Nucl. Sci., NS-29, 2018 (1982).

[6] K. LaBel, M. Gates, J. Barth, A. Johnston and P. Marshall, "Single event effect criticality analysis (SEECA)," Sponsored by NASA Headquarters/Code QW, http://radhome.gsfc.nasa.gov/radhome/papers/seecai.htm, Feb 15, 1996.

[7] M. A. McMahan, "Radiation effects testing at the 88-inch cyclotron," In Proceedings of the Fifth European Conference on Radiation and Its Effects on Components and Systems, RADECS 99, USA (1999), p.142, doi: 10.1109/RADECS.1999.858563.

[8] G. D. Alton and D. N. Smithe, "Design studies for an advanced ECR ion source," Rev. Sci. Instrum., vol. 65, no. 4, pp. 775–787, Apr. 1994.

[9] R. Geller, F. Bourg, P. Briand, J. Debernardi, M. Delaunay, B. Jacquot, P. Ludwig, R. Pauthenet (in memoriam), M. Pontonnier, and P. Sortais, "The Grenoble ECRIS status 1987 and proposals for ECRIS scalings," in Proc. 8th Workshop ECRIS, East Lansing, MI, 1987, p. 1.

[10] C. M. Lyneis, Z. Q. Xie, D. J. Clarck, R. S. Lam, and S. A. Lundgren, "Preliminary performance of the LBL AECR," In Proceedings of 10th International Workshop on ECR Ion Sources, Oak Ridge, TN, USA, 1990, 47.

[11] M. Kireeff Covo, J. Y. Benitez, A. Ratti, and J. L. Vujic, "Integrating a traveling wave tube into an AECR-U ion source," IEEE Trans. on Plasma Sci. 39 (2011) 1455, DOI: 10.1109/TPS.2011.2130542.

[12] C. M. Lyneis, Z. Q. Xie, and C. E. Taylor, "Design of the 3rd generation ECR ion source," In Proceedings of the 13th International Workshop on ECR Ion Sources, Texas A&M University, USA, 1997, 115.

[13] D.Z. Xie, J.Y. Benitez, A. Hodgkinson, T. Loew, C.M. Lyneis, L. Phair, P. Pipersky, B. Reynolds, and D. S. Todd. "Development status of a next generation ECRIS: MARS-D at LBNL," Rev. Scient. Instr. 87 (2016) 02A702, DOI: http://dx.doi.org/10.1063/1.4931713.

[14] M. Kireeff Covo, "Measurement of axial injection displacement with trim coil current unbalance," Rev. Scient. Instr. 85 (2014) 085113, DOI: http://dx.doi.org/10.1063/1.4892463.

[15] B. G. Harvey, Nuclear Spectroscopy and Reactions, Part A, Academic Press Inc., New York, 1974.

[16] D. Leitner, M. A. McMahan, D. Argento, T. Gimpel, A. Guy, J. Morel, C. Siero, R. Thatcher, C. M. Lyneis, "Heavy ion cocktail beams at the 88 Inch Cyclotron," Report LBNL-51451, 2002.

[17] M. Kireeff Covo, "Nondestructive synchronous beam current monitor," Rev. Scient. Instr. 85 (2014) 125106, DOI: http://dx.doi.org/10.1063/1.4902903.

[18] http://gretina.lbl.gov/

[19] K. E. Gregorich, "Simulation of recoil trajectories in gas-filled magnetic separators," Nucl. Instr. Meth. A711, 47 (2013)

[20] J. M. Gates, "Prospects of A and Z identification experiments at LBNL," Nobel Symposium NS 160 - Chemistry and Physics of Heavy and Superheavy Elements, Bäckaskog Castle, Sweden, Edited by Rudolph, D.; EPJ Web of Conferences, Volume 131, id.0800, December 2016, DOI: 10.1051/epjconf/201613108003

[21] M. A. McMahan, L. Ahle, D.L. Bleuel, L. Bernstein, B.R. Barquest, J. Cerny, L.H. Heilbronn, C.C. Jewett, I. Thompson, and B. Wilson, "Neutron beams from deuteron breakup at the 88-Inch Cyclotron at Lawrence Berkeley National Laboratory," ND2007, 411-414 (2007), DOI: 10.1051/ndata:07456

[22] D. L. Bleuel, M. A. McMahan, L. Ahle, B. R. Barquest, J. Cerny, L. H. Heilbronn, and C.C. Jewett, "Characterization of a tunable quasi-monoenergetic neutron beam from deuteron breakup," Nuclear Instruments and Methods in Physics Research Section B: Beam Interactions with Materials and Atoms, Volume 261, Issues 1–2, August 2007, Pages 974-979, ISSN 0168-583X, http://dx.doi.org/10.1016/j.nimb.2007.04.125.

[23] R. Beyer, R. Schwengner, R. Hannaske, A.R. Junghans, R. Massarczyk, M. Anders, D. Bemmerer, A. Ferrari, A. Hartmann, T. Kögler M. Röder, K. Schmidt, and A. Wagner, "Inelastic scattering of fast neutrons from excited states in ^{56}Fe," Nucl. Phys. A 927 (2014) 41-52

[24] A. Negret, C. Borcea, Ph. Dessagne, M. Kerveno, A. Olacel, A.J.M. Plompen, and M. Stanoiu, "Cross-section measurements for the ^{56}Fe(n,xnγ) reactions," PRC 90, 034602 (2014)

[25] http://www.micro-rdc.com/SEE%20Testing.htm